



Linking soil element-mass-transfer to microscale mineral weathering across a semiarid environmental gradient



Rebecca A. Lybrand*, Craig Rasmussen

Department of Soil, Water and Environmental Science, University of Arizona, 429 Shantz Building, #38, PO Box 210028, 1177 E. Fourth, Tucson, AZ 85721-0038, USA

ARTICLE INFO

Article history:

Received 17 October 2013

Received in revised form 24 April 2014

Accepted 29 April 2014

Available online 9 May 2014

Editor: Carla M. Koretsky

Keywords:

Feldspar

Critical zone

Mineral weathering

Granite

ABSTRACT

Understanding controls on silicate weathering is critical to characterizing critical zone evolution. The objective of this study was to investigate how climate, vegetation, and landscape position control feldspar transformations across a semiarid environmental gradient. Granitic surface soil and saprock samples were collected from desert scrub and mixed conifer sites within the Santa Catalina Mountain Critical Zone Observatory where mean annual temperature ranges from 24 °C to 10 °C and mean annual precipitation from 25 to 85 cm. Quantitative X-ray diffraction, X-ray fluorescence, and electron microprobe analyses were employed to quantify elemental changes in bulk soils and across plagioclase grains. The chemical depletion of Na in bulk soils ranged from 5.4 – 15% in the desert scrub sites relative to 16–33% in the mixed conifer sites. Plagioclase grain alteration was classified into unaltered, edge, and altered sections to compare microscale weathering and elemental variation. The Na/Al and Si/Al ratios decreased from unaltered, to edge, to altered grain sections in the mixed conifer sites, whereas the element ratios of the desert scrub system were similar between unaltered and edge grain sections, and only exhibited significant decreases in Na/Al and Si/Al ratios between edge and altered materials. The microscale depletion of Na and Si suggested increased silicate weathering in the cooler, wetter, and more biologically productive mixed conifer system compared to the hot, dry desert scrub system. The results also demonstrated a topographic control on mineral transformation where increased plagioclase weathering occurred in convergent footslope landscapes with little change in elemental depletion of soils in divergent summit sites.

© 2014 Elsevier B.V. All rights reserved.

1. Introduction

Silicate weathering and mineral transformations contribute significantly to landscape evolution and to our understanding of water and carbon cycling in the critical zone, which spans from the top of the vegetation canopy down to and including groundwater (NRC, 2001). Important questions remain regarding the role of various climatic, tectonic, and topographic factors in controlling silicate weathering mechanisms and microscale transformations in the critical zone. Here, we address how climate, vegetation, and landscape position interact to shape silicate weathering patterns through elemental loss in bulk soils and through microscale transformations of plagioclase feldspar grains.

The dominant controls on silicate weathering and the nature of the subsurface weathering front include water availability and temperature (White and Brantley, 1995; White et al., 1996; Dahlgren et al., 1997; White et al., 2001; Rasmussen and Tabor, 2007; Rasmussen et al., 2010), physical erosion (Riebe et al., 2001, 2004), and the interactions between climate and erosion (Jacobson et al., 2003; West et al., 2005;

Rasmussen et al., 2011). Additional factors reported to control extent and rates of silicate weathering include deep regolith and saprolite weathering (Dixon et al., 2009), vascular plants and primary production (Moulton et al., 2000), and topographic controls on soil production rates, mineral residence time, soil and solute transport distances, and soil depth (Heimsath et al., 1997; Green et al., 2006; Yoo et al., 2007; Yoo and Mudd, 2008). At the mineral scale, White and Brantley (2003) suggest that silicate weathering reaction rates are a product of both extrinsic properties, such as solute composition, climate, and/or biologic interactions, and intrinsic properties. Intrinsic properties can include increases in grain surface roughness and concurrent increases in mineral surface area or decreases in reactive surface area due to physical impediment by secondary weathering products or leached layers. Nearly all of these factors co-vary and interact, and thus present a challenge to understanding chemical weathering processes and critical zone evolution (Chorover et al., 2011).

The microscopic study of weathered mineral surfaces in the critical zone may be used to constrain the formation and distribution of secondary altered products, an aspect not readily addressed in laboratory investigations of feldspar weathering (Hochella and Banfield, 1995). Of the silicate minerals, feldspars comprise approximately 60% of the minerals in the Earth's crust (Kauffman and Van Dyk, 1994) and have been studied extensively in laboratory weathering experiments (e.g., Blum

* Corresponding author. Tel.: +1 760 271 5219 (mobile); fax: +1 520 621 1647.

E-mail addresses: rlybrand@email.arizona.edu (R.A. Lybrand), crasmuss@cals.arizona.edu (C. Rasmussen).

and Stillings, 1995). However, feldspar dissolution rates are consistently two to five orders of magnitude higher in laboratory settings compared to field studies (Blum and Stillings, 1995; White et al., 1996, 2001; White and Brantley, 2003; Zhu et al., 2006), likely a result of differences in mineral surface characteristics of freshly ground and naturally weathered feldspars. High-resolution imaging and accompanying chemical analyses present a powerful tool to investigate silicate weathering processes in critical zone systems that may help address this discrepancy, particularly in regard to the composition and mineral transformations that occur at reactive feldspar surfaces. Zhu et al. (2006) illustrated the ambiguous definitions associated with the feldspar surface–water interface that include but are not limited to: reactivity dominated by surface reactions between unaltered feldspar and the aqueous solution (Lagache, 1961); the occurrence of a cation deficient leached layer separating the reactive feldspar surface from aqueous solution (Paces, 1973); mineral dissolution controlled by non-diffusive, chemical reactions at the feldspar surface–water interface (Berner and Holdren, 1977, 1979); the existence of a sharp feldspar–amorphous silica chemical gradient created by interfacial dissolution–reprecipitation processes (Hellmann et al., 2003, 2012); or a complex surface where crystalline feldspar is separated from the aqueous solution by a thin (<10 nm) amorphous layer covered by discontinuous kaolinite and an outer layer of precipitated smectite. Similar to White and Brantley (2003), Zhu et al. (2006) related differences in feldspar reactivity of laboratory and field samples to intrinsic mineral properties including amorphous layer development and secondary mineral coatings on feldspars.

The objective of this work was to constrain how climate and vegetation, topographic position, and pedon depth control plagioclase weathering across a steep semiarid environmental gradient. Local environmental gradients that compress large climate and vegetation variation over short distances provide excellent opportunities to examine the interaction among these factors with minimal variation in bedrock and regional tectonics (Dahlgren et al., 1997). Plagioclase feldspar chemical composition in bulk soils was coupled with microscale elemental changes associated with feldspar chemical transformation. Electron microprobe wave dispersive spectroscopy (WDS) combined with backscattered electron (BSE) imagery was used to develop a classification scheme for characterizing the plagioclase grain–secondary mineral interface.

2. Methods

2.1. Field sites and sample collection

The two field sites, referred to here as *desert scrub* and *mixed conifer*, were sampled from the Santa Catalina Critical Zone Observatory environmental gradient in southern Arizona (Fig. 1a). These locations capture the relative end-members of the environmental gradient and encompass the largest variation in climate, vegetation, and topography. The Santa Catalina Mountains encompass significant range in temperature (10–24 °C) and precipitation (25–85 cm), with concurrent variation in vegetation community composition and structure (Whittaker and Niering, 1965; Whittaker et al., 1968; Table 1). Climate and vegetation both exert control on soil properties and silicate weathering, with distinct variation in soil development by vegetation community, or climate–vegetation zone (Whittaker et al., 1968). Additionally, local relief and topography vary significantly across the SCM (Pelletier et al., 2013), leading to landscape position variation in soil physical and chemical properties within each climate–vegetation zone (Lybrand et al., 2011).

A 1:125,000 digital spatial database containing geologic maps of the Catalina Core Complex and field observations of rocks were used to determine the geology of the field sites, which span two Tertiary-aged intrusive rock units (Dickinson, 1991, 2002). Specifically, the desert scrub site was located on the Oligocene–Miocene aged Catalina granitic pluton, and the mixed conifer site was located on the Eocene aged two-mica wilderness granite suite. The granitic parent materials exhibit

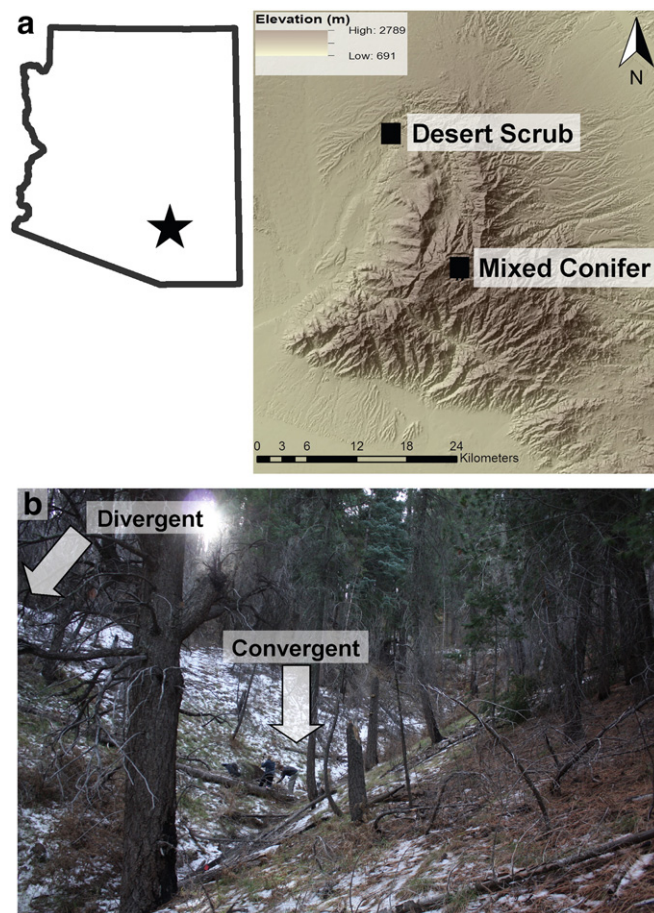


Fig. 1. a) Locations of the desert scrub and mixed conifer sites encompassed by the Santa Catalina Mountain environmental gradient in southern Arizona. b) An example of the two landscape positions studied in the project. The image is of an adjacent divergent–convergent landform unit pair at the mixed conifer field site.

similar mineral and elemental composition except for the dominant mica mineral where the desert scrub site is dominated by biotite and the mixed conifer location is dominated by muscovite (Table 2).

Local topographic controls on silicate weathering were examined in the desert scrub and mixed conifer systems by sampling a combination of divergent summit landscape positions and adjacent convergent footslope positions. The divergent summit positions are a source of soil materials and solutes to adjacent convergent footslope sites where increased water availability and colluvial inputs likely enhance silicate weathering and mineral transformation (Huggett, 1975; Birkeland, 1999). The sample location design follows similar hillslope scale soil studies that focus on the interactive control of climate and topography on granitic soil development (Watson, 1964; Muhs, 1982; Khomo et al., 2011).

Soil, saprock, and representative parent rock samples were collected from the desert scrub and mixed conifer locations (Fig. 2a, b). Pedons were excavated to the depth of refusal from north-facing convergent and divergent landscape positions for a total of four pedons per sample location. Pedon locations were selected based on field observations of local topography and landscape configuration. Soils and saprock were sampled by morphologic horizon and described using established methods (Schoeneberger et al., 2011). Soil subgroup classifications and dominant vegetation were also determined for each field site (Table 1). The weathered parent material observed at the sites in the current study best matched the characteristics of saprock as outlined by Graham et al. (2010), where saprock is defined as weathered parent material that retains the structural features of the parent rock, can be broken apart with bare hands, and is dominated by primary minerals

Table 1
Site and soil properties for the desert scrub and mixed conifer soil pedons. Soil pH, pedon soil organic carbon (SOC), and depth to paralithic contact are reported as depth-weighted averages $\pm 2\sigma$.

Field site	Landscape position	Elevation (m)	MAT (°C)	MAP (cm)	MAP/PET ratio	1:1 soil: water pH $\pm 2\sigma$	1:1 soil: 1 M KCl pH $\pm 2\sigma$	Pedon SOC (kgm^{-2}) $\pm 2\sigma$	Depth to paralithic contact (cm) $\pm 2\sigma$	Soil subgroup classification	Dominant vegetation type
Desert scrub	Convergent	1081	18.1	18.1	0.4	6.2 \pm 0.38	5.0 \pm 0.94	3.7 \pm 2.3	39 \pm 2.8	Typic Torriorthent	Saguaro (<i>Carnegiea gigantea</i>), Ocotillo (<i>Fouquieria splendens</i>), Acacia, Arizona
Desert scrub	Divergent	1081	18.1	18.1	0.4	6.2 \pm 0.00	4.8 \pm 0.10	1.2 \pm 0.20	10 \pm 2.8	Typic Torriorthent	Barrel Cactus (<i>Ferocactus wislizeni</i>), and Agave (<i>Agave schottii</i> , <i>Agave palmeri</i>)
Mixed conifer	Convergent	2410	9.4	95.4	1.2	5.6 \pm 0.70	4.3 \pm 0.46	17 \pm 0.14	100 \pm 28	Typic Ustorthent	Douglas fir (<i>Pseudotsuga menziesii</i>), ponderosa pine (<i>Pinus ponderosa</i>) and white fir (<i>Abies concolor</i>)
Mixed conifer	Divergent	2410	9.4	95.4	1.2	5.7 \pm 1.1	4.4 \pm 1.2	8.7 \pm 0.04	59 \pm 4.2	Typic Ustorthent	

that have not undergone extensive chemical alteration to secondary products.

2.2. Sample characterization

2.2.1. Soil chemical properties

All soils were air-dried, and sieved at <2 mm to isolate the “fine-earth” fraction for analyses (Soil Survey Staff, 2004). Soil pH was determined for all soil samples using 1:1 soil:water and 1:1 soil:1 M KCl extracts (Soil Survey Staff, 2004). Soil organic carbon (SOC) was measured by the University of Arizona’s Environmental Isotope Laboratory using a Finnigan Delta Plus XL (Thermo Fisher Scientific, Bremen, Germany) coupled to an elemental analyzer (Costech Analytical Technologies Inc., Valencia, CA, USA). The soil properties, including pH, SOC, and depth to paralithic contact, were reported as depth-weighted pedon averages ± 2 standard deviations (2σ) (Table 1).

2.2.2. Mineralogical and elemental composition

Quantitative X-ray diffraction (QXRD), X-ray fluorescence (XRF), and electron microprobe analyses were used to quantify mineral type and abundance, bulk soil elemental distribution, and parent rock composition of all samples. Additionally, a total of four surface and saprock samples from each of the divergent summit landscape positions at the desert scrub and mixed conifer locations were subsampled for micro-scale characterization of plagioclase grain transformations using an electron microprobe (Fig. 2a, b). The surface samples were collected from the topmost mineral horizon that spanned 0 to 3 cm for the desert scrub site and 0 to 4 cm for the mixed conifer site. The saprock samples were collected from the uppermost paralithic contact within each field

site, which occurred at ~10 cm in the desert scrub site and ~35 cm in the mixed conifer site. Plagioclase minerals were the focus of the

Table 2
The mineral assemblage, weight percent ($\pm 2\sigma$), and associated mineral formulas of the parent rock collected from the field sites. Mineral formulas were also calculated for muscovite grains in mixed conifer soil, biotite grains in desert scrub soil, and biotite in desert scrub dust. The $\pm 2\sigma$ does not account for analytical error ($\pm 5\%$ relative).

Mineral	Weight (%)	CV (%)	Mineral formula
<i>Mixed conifer (site coordinates: 32.429009° N, -110.770223° W)</i>			
Muscovite (rock)	11 \pm 3.2	15	$\text{K}_{0.902}\text{Mg}_{0.095}\text{Fe}_{0.323}\text{Al}_{2.554}\text{Si}_{3.115}$
Muscovite (soil)	14 \pm 3.5	13	$\text{K}_{0.967}\text{Mg}_{0.114}\text{Fe}_{0.318}\text{Al}_{2.483}\text{Si}_{3.144}$
Oligoclase	38 \pm 5.8	7.5	$\text{K}_{0.011}\text{Na}_{0.857}\text{Ca}_{1.02}\text{Al}_{1.111}\text{Si}_{2.899}$
Microcline	19 \pm 1.7	4.4	$\text{K}_{0.887}\text{Na}_{0.082}\text{Ca}_{0.002}\text{Al}_{1.022}\text{Si}_{2.989}$
Quartz	32 \pm 4.2	6.5	SiO_2^a
<i>Desert scrub (site coordinates: 32.555829° N, -110.841022° W)</i>			
Biotite (rock)	3 \pm 2.4	39	$\text{K}_{0.695}\text{Mg}_{1.433}\text{Fe}_{0.960}\text{Al}_{1.498}\text{Si}_{2.852}$
Biotite (soil)	7 \pm 3.1	23	$\text{K}_{0.800}\text{Mg}_{1.509}\text{Fe}_{0.897}\text{Al}_{1.166}\text{Si}_{2.984}$
Biotite (dust)	–	–	$\text{K}_{0.603}\text{Mg}_{1.148}\text{Fe}_{0.8895}\text{Al}_{1.627}\text{Si}_{2.975}$
Oligoclase	37 \pm 17	24	$\text{K}_{0.029}\text{Na}_{0.814}\text{Ca}_{1.20}\text{Al}_{1.124}\text{Si}_{2.883}$
Orthoclase	28 \pm 12	21	$\text{K}_{0.862}\text{Na}_{0.121}\text{Ca}_{0.002}\text{Al}_{1.011}\text{Si}_{2.989}$
Quartz	32 \pm 10	16	SiO_2^a

^a Ideal mineral formula (formula not calculated during this study).

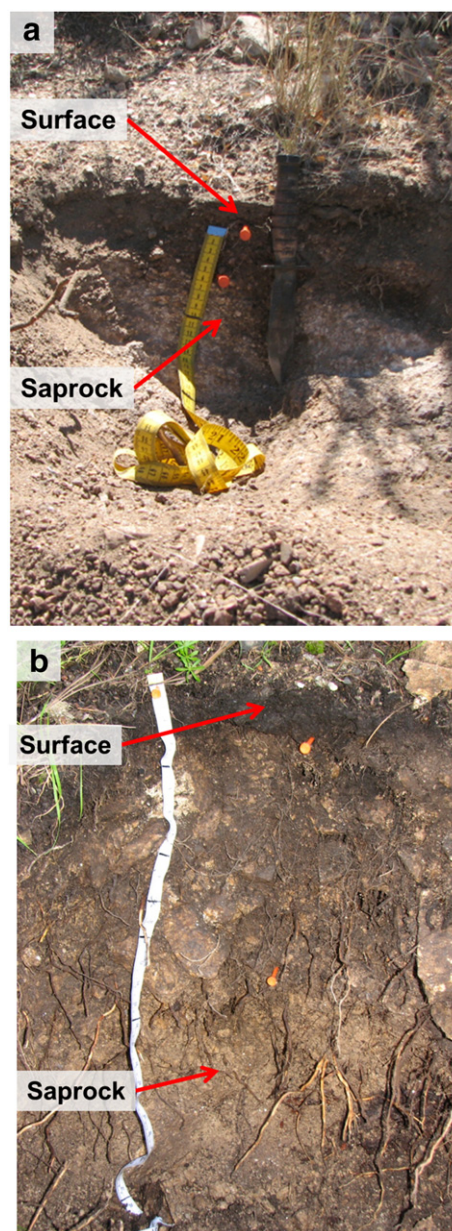


Fig. 2. A schematic of sample locations in a) the desert scrub divergent pedon and b) the mixed conifer divergent pedon.

microscale quantification part of this study because the parent rocks of both study areas contained comparable amounts of these minerals (Section 3.1). Plagioclase feldspars are also one of the first primary minerals to undergo chemical transformation, making the impacts of climate and vegetation easier to distinguish and quantify (White et al., 2001; Papoulis et al., 2004).

Parent rock mineral composition and mineral formulas were calculated using elemental weight percentages determined by microprobe point analyses. Representative unweathered rock fragments were fixed in 2.5 cm round Araldite epoxy mounts and finely polished (grit size of 0.5 μm). The rock mounts were analyzed at the University of Arizona Electron Microprobe Laboratory using a CAMECA SX50 Ultra electron probe microanalyzer (EPMA). Instrument conditions were set to a 15 kV accelerating voltage, an electron beam size of 2 μm , and a 20 nA current for all elements except Na and K where an 8 nA current was used to prevent alkali migration. Parent rock mineral formulas were calculated with the Spear normalization technique (Spear, 1993) and aided in the selection of the closest matching mineral patterns from the RockJock Library and the American Mineralogist Crystal Structure Database (Downs and Hall-Wallace, 2003) to improve QXRD accuracy for assessing mineral assemblage and abundance.

Soils were pre-treated prior to QXRD and microprobe analysis to remove organic matter using NaOCl adjusted to pH 9.5 (Soil Survey Staff, 2009). The soils were ground to <355 μm using a mortar and pestle. A known amount of zincite was added to the ground soil as an internal standard and micronized into a homogenous, bulk powder (<180 μm) using a McCrone Micronizing Mill (Moore and Reynolds, 1997; Eberl, 2003). Rocks were broken using a mallet, or a sledgehammer when necessary, and internal, un-weathered fragments were selected from the specimen centers. Rock fragments were ground and processed using the same methods described for soils. Clays were prepared as oriented clay mounts on glass slides using a vacuum filtration technique (Moore and Reynolds, 1997). The clay mounts underwent standard treatments to aid in secondary mineral identification including K-saturation (KCl–25 °C, KCl–300 °C, and KCl–550 °C), Mg-saturation (Mg–25 °C), Mg/glycerol saturation (Mg–Gly–25 °C), and a formamide treatment to differentiate halloysite from kaolinite (Churchman et al., 1984).

Oriented clay mounts and randomly oriented, bulk soil and rock powder mounts were analyzed by X-ray diffraction at the University of Arizona's Center for Environmental Physics and Mineralogy with a PANalytical X'Pert PRO Multi-Purpose Diffractometer (PANalytical, Almelo, The Netherlands). The system generated Cu-K α X-rays at an accelerating potential of 45 kV, a current of 40 mA, and was equipped with a 1° divergence slit (1.52 mm), a 10 mm divergent mask, a 1° anti-scatter slit (1.52 mm), a 0.60 mm fixed receiving slit, and a sealed Xenon detector fitted with a graphite monochromator. A spinner sample stage with a 1 s rotation time was used to measure from 4 to 65° 2-theta, with a step size of 0.020° and a dwell time of 3 s. Semi-quantitative X-ray diffraction was employed to determine secondary mineral assemblage where a fixed sample stage was used to measure oriented clay mounts with a scan range of 2–35° 2-theta, a step size of 0.040° and a dwell time of 3 s. The diffractometer was fitted with a 1° divergence slit (1.52 mm), a 10 mm divergent mask, a 1° anti-scatter slit (1.52 mm), a 0.60 mm fixed receiving slit, and a sealed Xenon detector with a graphite monochromator.

Quantitative phase analysis of the bulk soil and rock samples was completed using the full-pattern fit Rietveld refinement method (Bish and Post, 1993; Bish, 1994), an extension of the Rietveld method (Rietveld, 1969). The Rietveld method uses a least squares minimization process that relies on a set of user-defined crystal structure refinements to minimize differences between the observed diffraction pattern and the reference mineral patterns. The Rietveld refinements were performed in PANalytical X'Pert HighScore Plus v2.1b using reference mineral patterns from the RockJock Library and the American Mineralogist Crystal Structure Database (Downs and Hall-Wallace, 2003). The

parameters selected for the refinement strategy sequence were based on Young's (1993) suggested parameter sequence. A set of global parameters, including R expected, weighted R, and goodness of fit generated by the software, were used to evaluate each refinement to ensure the production of accurate, high quality data (Speakman, 2013). Mineral phase quantification was independently confirmed by analyzing a subset of the rock and soil samples in RockJock (Eberl, 2003). Characteristic secondary minerals were identified using HighScore Plus with reference mineral patterns from the RockJock Library and the American Mineralogist Crystal Structure Database.

Major, minor, and trace elemental constituents were determined by XRF for all soil and rock samples. Soils were prepared by ball milling ~3.5 g of sample in a plastic scintillation vial containing 3 tungsten carbide bearings for 10 min. Internal rock fragments were ground to <355 μm using a porcelain mortar and pestle. The ground soil and rock samples were formed into pellets under a pressure of 25 tons for 120 s, bound with cellulose wax (3642 Cellulose binder – SPEX SamplePrep PrepAid™), and analyzed using a Polarized Energy-Dispersive X-ray Fluorescence spectrometer (EDXRF–SPECTRO XEPOS, Kleve, Germany). The XRF concentrations measured for soils were corrected for loss on ignition and reported on an ash free basis. Loss on ignition was determined by weighing out 20 g of dried (105 °C for 24 h), un-treated soil, placing the sample in a muffle furnace for 3 h at 550 °C, cooling the sample in a desiccator, and re-weighing the sample post-ignition. Loss on ignition was then calculated as the percent of dry weight that was lost on ignition (Konen et al., 2002).

The relative Na mass transfer was calculated for each soil horizon using quartz and Na as the immobile and mobile constituents, respectively. Sodium was used as a proxy for plagioclase weathering (Rasmussen et al., 2011) because Na bioaccumulation in the soil is generally low (<1%), making Na loss from transforming feldspars more quantifiable than other elements (White and Brantley, 2003). Quartz was selected as a conservative component because of its consistent distribution in the parent rock (White et al., 1996) and its demonstrated similarity in immobility to conservative elements, such as Zr and Ti (Jin et al., 2010). The degree of elemental loss or gain was determined using the dimensionless mass transfer coefficient, $\tau_{i,j}$, following Porder et al. (2007):

$$\tau_{i,j} = \left[\frac{c_{j,w} c_{i,p}}{c_{j,p} c_{i,w}} - 1 \right] \times [1 - \text{RF}\%] \quad (1)$$

where $c_{j,p}$ and $c_{i,p}$ are concentrations of the mobile and immobile constituents in the parent material, $c_{j,w}$ and $c_{i,w}$ are soil concentrations, and RF% is weight percent rock fragments.

2.3. Microscale characterization

Rock, saprock, and soil mineral arrangement and composition were studied using an electron microprobe to produce backscattered electron images, element X-ray maps, and point elemental weight percentages of mineral grains (Hill and Sawhney, 1971; Ghabru et al., 1987; Dixon et al., 2006; Sedov et al., 2008). Following previous studies of granitic mineral transformations, including those of feldspar (Zhu et al., 2006; Lee et al., 2008; Plummer and Putnis, 2009) and mica (Fordham, 1990; Robertson and Eggleton, 1991), the microprobe technique was applied to differentiate chemical weathering processes, specifically primary minerals and secondary weathering products (Sequeira Braga et al., 2002; Driese et al., 2007).

Four pre-treated subsamples of the fine-earth soil fraction and saprock were prepared for microprobe analysis. Approximately 0.1 g of bulk fine-earth sample was mounted in a 1" round Araldite epoxy mount and polished to a final grit size of 0.5 μm . The samples were analyzed at the University of Arizona Electron Microprobe Laboratory

using a CAMECA SX100 Ultra EPMA that was calibrated using a set of silicate mineral standards.

Ten plagioclase feldspar grains were randomly selected within each mounted sample for characterization and elemental analysis. The grains ranged in size from $<50\ \mu\text{m}$ to $\sim 200\ \mu\text{m}$ in length. Backscattered electron images of the grains revealed heterogeneous weathering patterns that were classified as: (1) unaltered, (2) edge, and (3) altered (Fig. 3a, b). The unaltered sections were defined as grain areas exhibiting smooth surfaces with no apparent evidence of weathering (i.e. dissolution pitting, fracturing, etc.) and no elemental loss (total element weight $\sim 100\%$). The edge classification was assigned to any grain area $\sim 2\text{--}3\ \mu\text{m}$ from the grain edge or fracture where the degree of alteration and total elemental weight percentages were variable ($>70\%$ – 100%). Altered grain areas appeared darker due to a greater abundance of heavier Si and Al atoms and were located in grain fractures and along edges. Altered grain areas contained variable total elemental weight percentages ($>70\%$) and were dominated by weathering products. The classification scheme was designed to account for changes in the degree of grain transformation occurring among sample locations (Fig. 3a, b).

Mineral composition of the unaltered grain areas was quantified using a combination of randomly selected point analyses and horizontal/vertical straight line transects with point analyses taken every $\sim 10\text{--}15\ \mu\text{m}$. The microprobe conditions for unaltered grain point analyses included an electron beam size of $2\ \mu\text{m}$ and a $20\ \text{nA}$ current for all elements except Na and K where an $8\ \text{nA}$ current was used. Grain edges and altered materials were quantified with point analyses using the electron microprobe specifications described by Velde (1984) for clay mineral analysis ($2\ \mu\text{m}$ beam size and a $2\ \text{nA}$ current). All analyses were conducted at $15\ \text{kV}$.

A set of elemental data (Na, K, Al, Mg, Si, Ca, Ti, Cr, Fe, Mn and P) were produced for every microprobe point analysis made. A minimum of 5 and up to 20 points were analyzed and averaged per classification type (i.e., unaltered, edge, and altered) across every plagioclase feldspar grain examined in the study. A total of 10 plagioclase feldspar grains were analyzed per bulk sample. Microscale chemical composition of grain sections was examined using elemental ratios relative to Al,

including Na/Al, Si/Al, K/Al, Fe/Al, and Mg/Al, as general proxies for relative element loss (Birkeland, 1999).

Two-sample t-tests were performed in SigmaPlot (v. 12, Systat Software, Inc.) on log-transformed elemental weight percentages obtained from the microprobe point analyses. The t-tests were used to test for significant differences among the grain classes, the mixed conifer and desert scrub field sites, and to compare surface soils to saprock samples. The sample variables, t-statistics, degrees of freedom, and P-values were reported for every t-test completed (Table A1).

3. Results

3.1. Parent material composition

Parent rock composition of the two field sites was similar in mineral abundance, calculated mineral formulas, and primary mineral assemblage, except for the dominant type of mica (Table 2). All major primary mineral percentages fell within $\pm 10\%$ of one another across locations. Oligoclase was the dominant plagioclase mineral with Na/Ca molar ratios ranging from 6.8 to 8.4 in the desert scrub and mixed conifer sites, respectively. The remaining oligoclase element compositions of the desert scrub minerals were similar to the mixed conifer minerals (Table 2). Oligoclase and microcline weight percentages from the desert scrub rocks ranged from 28–48% and 18–32% versus the mixed conifer parent rocks that contained respective ranges of 33–40% and 18–20%. Quartz comprised 24–37% of the desert scrub parent rock compared to 29–34% in the mixed conifer parent rock. The primary difference between the parent rocks was that biotite (1–4%) was the predominant mica mineral in the desert scrub site whereas muscovite (9–13%) was prevalent in the mixed conifer site (Table 2). The desert scrub biotite contained an average of 0.697 mol K, 1.433 mol Mg, and 0.960 mol Fe in contrast to 0.902 mol K, 0.095 mol Mg and 0.323 mol Fe in the mixed conifer muscovite.

Biotite grains were examined in the parent rock, soil, and dust samples at the desert scrub site (Table 2). Dust was collected in four dust traps installed at the desert scrub location that were similar in

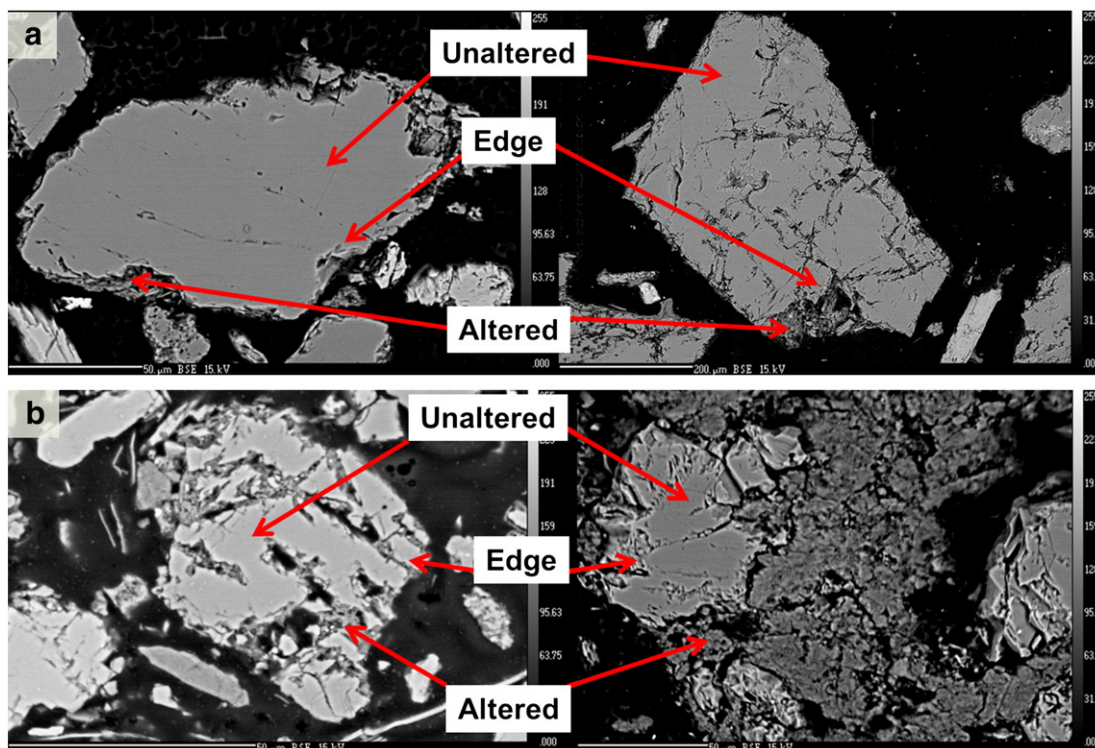


Fig. 3. Backscattered electron images documenting how a) desert scrub and b) mixed conifer plagioclase feldspar grains were classified consistently across field sites.

construction to those described by Reheis and Kihl (1995). Soil biotite grains tended to show enrichment in K and Mg relative to the rock and dust samples, with ~0.2 mol K difference between the biotite grains in the soil and dust and ~0.36 mol greater Mg in the soil compared to the dust. Conversely, Fe in the biotite varied little (~0.07 mol) among the rock, soil, and dust.

3.2. Soil chemical and mineralogical characterization

3.2.1. General soil chemical properties

The desert scrub and mixed conifer soils differed in terms of pH, SOC content, and secondary mineral assemblage (Table 1, Fig. 4a,b). The pH values of the soil–water extracts averaged 6.2 in desert scrub horizons compared to 5.6 in mixed conifer soil horizons (Table 1). The KCl pH values averaged 4.9 in desert scrub soils relative to an average of 4.3 in the mixed conifer soils. The highest average SOC content of 17 kg m⁻² was observed in the mixed conifer convergent soils, whereas the lowest SOC content of 1.2 kg m⁻² was observed in the desert scrub divergent landscapes. The clay mineral assemblage of the desert scrub location included vermiculite, smectite, hydrated halloysite, dehydrated halloysite and/or kaolinite (Fig. 4a). Conversely, the mixed conifer clay minerals generally included vermiculite, hydroxy-interlayered vermiculite (HIV), illite, and kaolin, with lesser amounts of hydrated halloysite, smectite, and gibbsite (Fig. 4b).

3.2.2. Bulk soil Na depletion

Chemical depletion of Na was observed in both the desert scrub and mixed conifer sites (Fig. 5a, b). Sodium chemical loss was most

consistent with depth in the mixed conifer system with the convergent horizons exhibiting average Na losses of 25% (n = 13) relative to adjacent divergent soil horizons with an average of 8.9% loss (n = 7). The maximum Na depletion of 33% was observed in the convergent surface horizon, whereas only 6.5% Na loss was observed in the convergent saprock material (Fig. 5b). In contrast, the desert scrub sites exhibited less distinction in Na loss between landscape positions where maximum chemical depletion was 5.4% in the divergent horizons and 15% in the convergent horizons. Desert scrub divergent soil horizons averaged 2.9% Na loss (n = 6) relative to 3.2% (n = 8) in the convergent horizons.

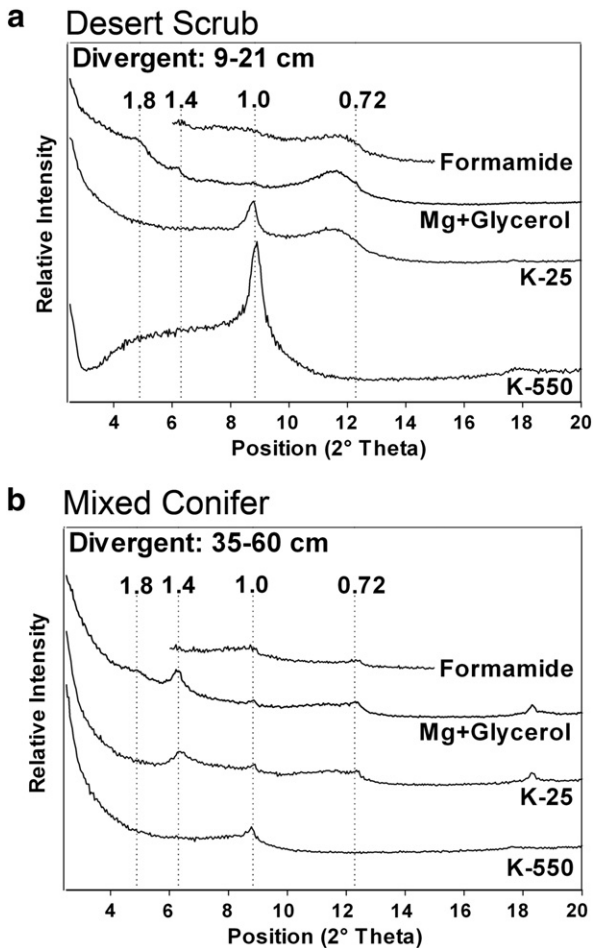


Fig. 4. X-ray diffractogram patterns of clay fractions from a) desert scrub and b) mixed conifer divergent saprock samples.

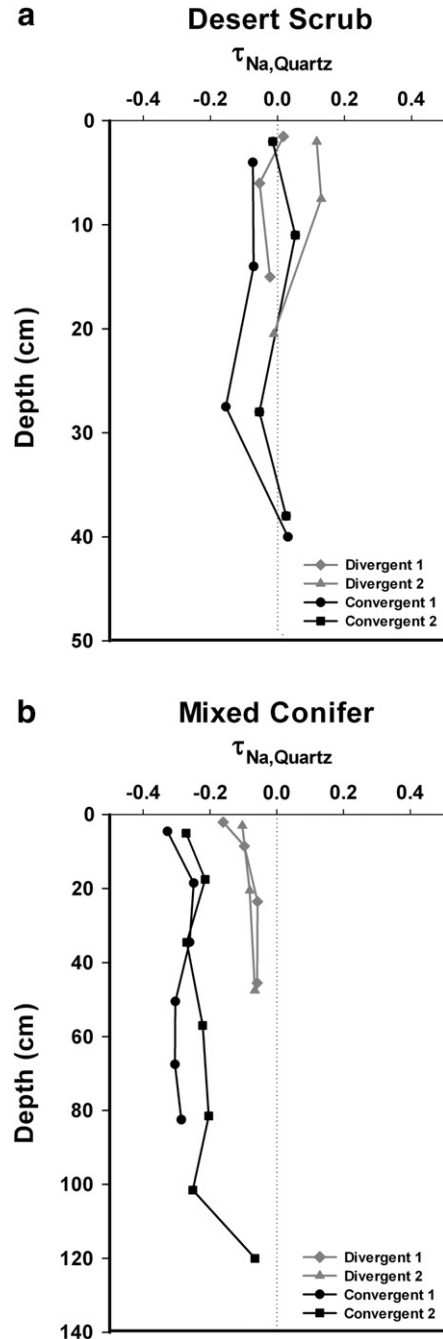


Fig. 5. Changes in Na weight percent relative to the immobile reference element, quartz (SiO₂). The figures highlight Na depletion across landscape positions in a) the desert scrub and b) mixed conifer sites.

3.3. Microscale feldspar weathering

3.3.1. Chemical depletion of Na and Si

Plagioclase grains in the mixed conifer surface soils exhibited a significant ($P < 0.001$) decrease in Na/Al from unaltered to altered grain sections (Fig. 6c, d; Table 3). The Na/Al coefficient of variation (CV) for mixed conifer surface grains was ~6.5 times greater in the altered sections compared to measurements made for the unaltered sections (Table 3). A similar trend was noted for the saprock plagioclase grains where Na/Al decreased significantly from unaltered to altered grain sections (Fig. 6d; Table 3), and the CV increased five-fold from unaltered to altered grain sections. The CV of the surface edge sections was ~1.5 times higher than the saprock edge measurements, suggesting less edge heterogeneity in Na loss with depth.

The Na/Al ratios for unaltered and edge sections in desert scrub plagioclase grains were similar (Fig. 6a, b), yet a significant decrease in Na/Al was observed between edge and altered grain sections (Tables 3, A1). In the surface horizons, Na/Al decreased minimally from unaltered to edge grain sections and decreased four-fold from edge to altered grain sections (Table 3). Surface grain CV values increased ~60% from unaltered to altered sections. Similarly, saprock Na/Al exhibited minimal decrease from the unaltered to edge sections, but decreased nearly 5-fold from edge to altered sections (Fig. 6b). The CV percentages increased by ~47% from unaltered to altered grain sections (Table 3). Highly significant differences in Na/Al were noted for edge to altered section comparisons in both surface and saprock samples but not for Na/Al comparisons between unaltered and edge sections (Table A1).

Similar to Na/Al, Si/Al values decreased significantly ($P < 0.001$) between unaltered and altered sections of mixed conifer plagioclase

grains (Tables 3, A1). The Si/Al for both surface and saprock grains decreased from unaltered, to edge, to altered grains, indicating increased desilication with grain transformation (Fig. 7c, d; Table 3). The CV values in surface and saprock samples were lowest in the unaltered grain sections followed by edge and then altered grain areas (Table 3). The edge sections were significantly different ($P < 0.001$, Table A1) from altered grain sections in both the surface and saprock samples.

In contrast to the mixed conifer location, desert scrub Si/Al values of surface and saprock grains were relatively homogeneous across grain sections (Fig. 7a, b). Desert scrub surface grains contained similar Si/Al ratios in unaltered and edge grain sections and exhibited a decrease of only ~1 unit in the altered materials (Table 3). Similarly, there was little change in Si/Al in unaltered and edge saprock grain sections and only a slight decrease observed in the altered grains (Fig. 7b, Table 3). The CV values increased more than three-fold from unaltered to altered sections in both desert scrub surface and saprock grains (Table 3). Unaltered grain sections were significantly different than altered grain sections in both surface and saprock horizons ($P = 0.005$ and $P < 0.001$, respectively).

3.3.2. Enrichment of K, Fe, and Mg in desert scrub altered materials

Observed K/Al values were < 0.1 in all samples (grain, edge, and altered) except for the altered materials on the desert scrub surface grains where K/Al values averaged 0.16 and indicated a relative K enrichment (Fig. 8a–d, Table 3). The K/Al values calculated for desert scrub surface biotite grains overlapped with those of plagioclase altered grain sections (Fig. 9a). The altered sections of the desert scrub surface plagioclase grains were also enriched in Fe (Fig. 9b) and Mg (Fig. 9c). The Fe/Al and Mg/Al ratios of the plagioclase altered grain sections overlap with

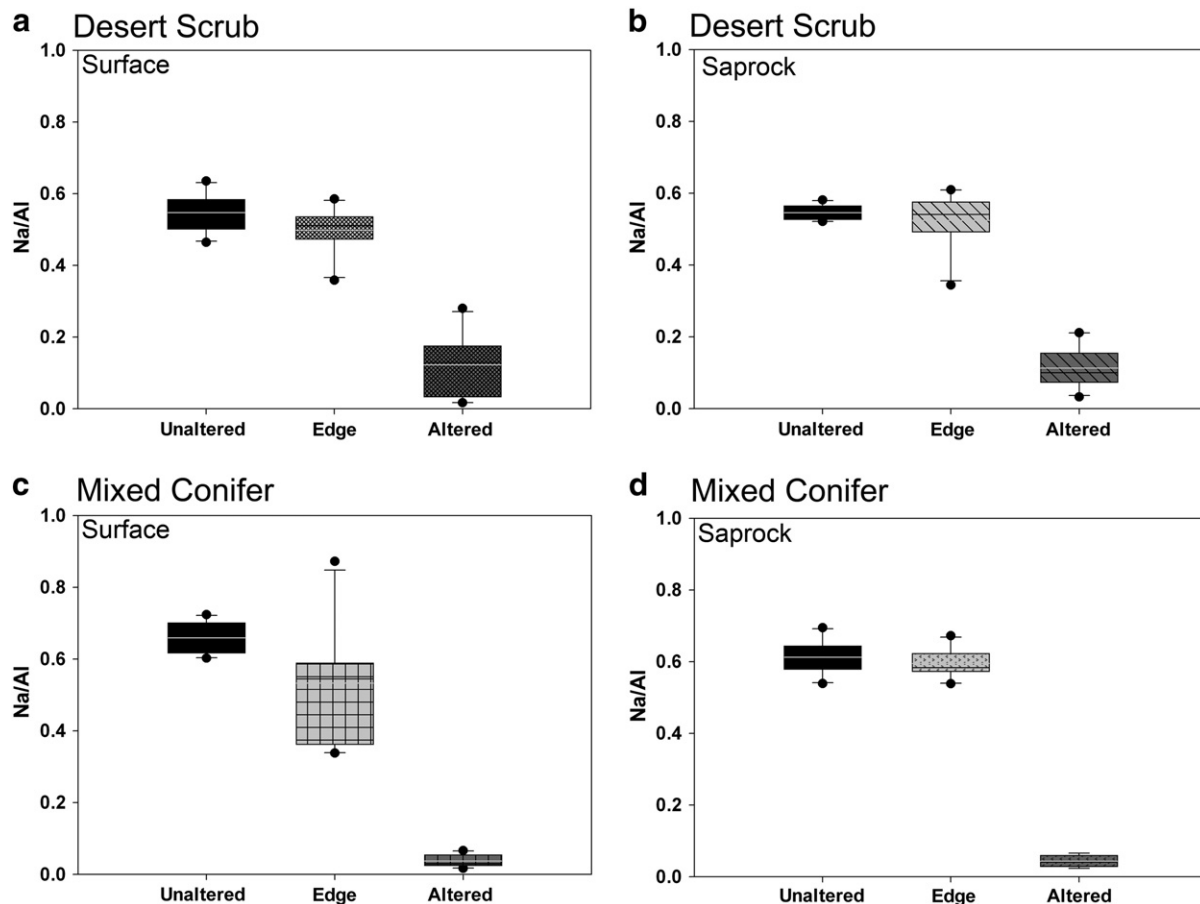


Fig. 6. Box plots summarizing Na/Al ratio averages for grains analyzed in the a) desert scrub surface soil, b) desert scrub saprock, c) mixed conifer surface soil, and d) mixed conifer saprock. Each box plot is composed of 10 data points analyzed for each classification scheme (i.e., unaltered).

Table 3The Na/Al, Si/Al, and K/Al ratio averages $\pm 2\sigma$, and coefficient of variation (CV %) for the sites, soil depths, and grain sections studied in the project.

Soil depth	Grain section	Avg. Na/Al	CV (%)	Avg. Si/Al	CV (%)	Avg. K/Al	CV (%)
<i>Mixed conifer</i>							
Surface	Unaltered	0.66 \pm 0.08	6.5	2.6 \pm 0.22	4.4	0.02 \pm 0.01	24
Surface	Edge	0.53 \pm 0.34	32	2.5 \pm 0.6	12	0.04 \pm 0.06	73
Surface	Altered	0.04 \pm 0.032	44	1.5 \pm 0.48	16	0.05 \pm 0.09	85
Subsurface	Unaltered	0.61 \pm 0.08	8.0	2.5 \pm 0.26	5.3	0.01 \pm 0.00	13
Subsurface	Edge	0.60 \pm 0.08	6.6	2.6 \pm 0.42	8.0	0.01 \pm 0.00	14
Subsurface	Altered	0.04 \pm 0.06	41	1.5 \pm 0.56	19	0.03 \pm 0.04	62
<i>Desert scrub</i>							
Surface	Unaltered	0.55 \pm 0.11	9.0	2.4 \pm 0.26	5.4	0.03 \pm 0.02	27
Surface	Edge	0.50 \pm 0.12	13	2.4 \pm 0.3	6.4	0.04 \pm 0.02	37
Surface	Altered	0.12 \pm 0.16	68	2.1 \pm 0.66	16	0.16 \pm 0.34	105
Subsurface	Unaltered	0.55 \pm 0.04	3.7	2.4 \pm 0.08	1.8	0.03 \pm 0.01	19
Subsurface	Edge	0.52 \pm 0.16	15	2.6 \pm 0.38	7.5	0.06 \pm 0.12	86
Subsurface	Altered	0.11 \pm 0.12	51	1.9 \pm 0.5	13	0.07 \pm 0.04	29

the lower end of ratios calculated for a desert scrub biotite grain (Fig. 9b, c), which was located adjacent to a plagioclase grain examined in this study (Fig. 9d). Point analyses shown in the altered biotite column (Fig. 9a–c) include unaltered biotite grain sections and fully transformed secondary clay products analyzed in the expanded interlayer space (Fig. 9d, e).

The morphology of the altered materials associated with the desert scrub plagioclase grains presented as clay films (Fig. 10a–c) in contrast to mixed conifer altered materials that presented a morphological appearance of in situ transformation products (Fig. 11a, b). Clay films in the desert scrub system were identified as altered materials coating primary mineral grains and were noted on all desert scrub plagioclase grains. Frayed-edge biotite grains were observed in desert scrub surface

soil (Figs. 9d, e; 12a, c), saprock (Fig. 12b), and dust (Fig. 12d), suggesting potential elemental contributions from weathered biotite to clay films on the plagioclase grains.

4. Discussion

4.1. Controls and variation in plagioclase weathering

4.1.1. Climate and vegetation

Greater bulk soil Na depletion with increased elevation may be attributed to a combination of greater moisture availability and biological production at higher elevations. The annual water budget shifts from water-limited in the desert scrub system where mean annual

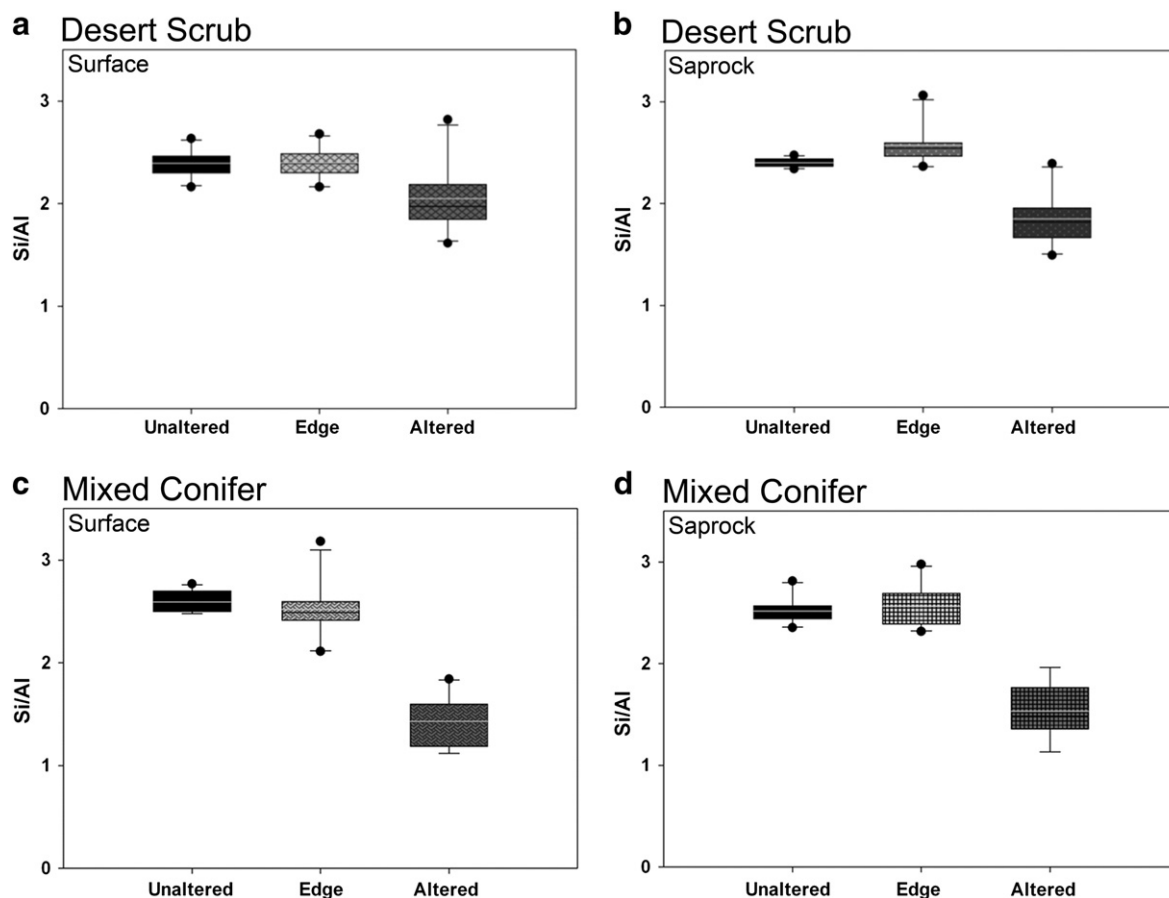


Fig. 7. Box plots documenting Si/Al ratios measured for plagioclase grains in a) desert scrub surface soil, b) desert scrub saprock, c) mixed conifer surface soil, and d) mixed conifer saprock.

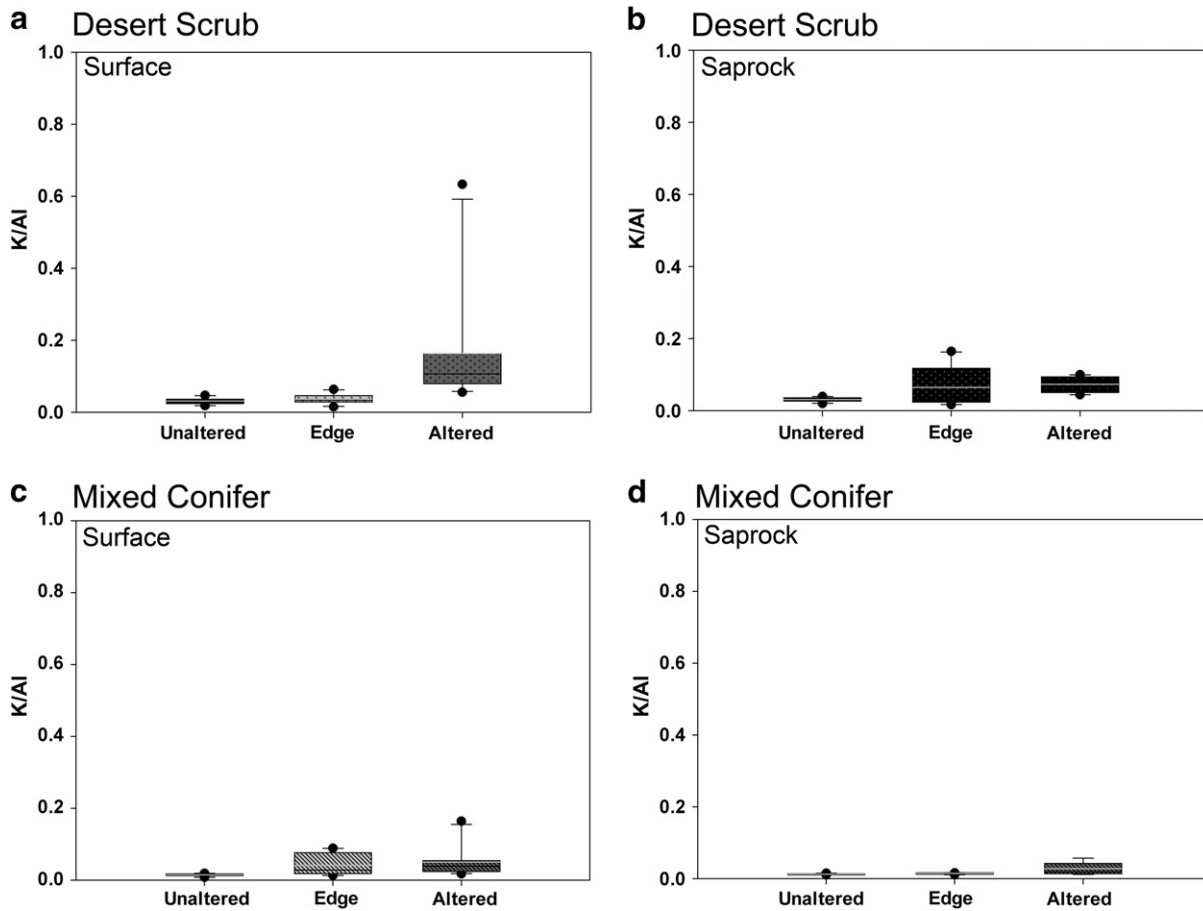


Fig. 8. Box plots detailing K/AI ratios in plagioclase grain sections from the a) desert scrub surface soil, b) desert scrub saprock, c) mixed conifer surface soil, and d) mixed conifer saprock.

precipitation (MAP) is less than potential evapotranspiration (PET) with a MAP/PET ratio of ~ 0.4 , to energy-limited in the mixed conifer system where precipitation exceeds the energy available to drive potential evapotranspiration with MAP/PET of ~ 1.2 to 1.4 (Budyko, 1974). The mixed conifer sites thus have annual precipitation inputs in excess of evapotranspiration that are available to leach through the soil, participate in chemical weathering reactions, and remove reaction products from the soil system. The patterns observed here were similar to chemical depletion relationships to water availability noted in previous work (Egli et al., 2003; Williams et al., 2010; Rasmussen et al., 2011). In particular, the magnitude of change in surface tau Na values from roughly -0.1 to -0.4 relative to increasing water availability observed in the SCM was very similar to the magnitude of change in Na loss noted in a broad synthesis of locations presented by Rasmussen et al. (2011).

Concurrent with changes in temperature and water availability in the SCM are changes in biological production, the amount of reduced carbon entering and being stored in the soil system, and soil pH (Whittaker and Niering, 1975). Vegetation assemblage transitions from desert scrub, with limited biological production on the order of $\sim 90 \text{ g m}^{-2} \text{ yr}^{-1}$ and relatively little canopy cover at low elevation, to mixed conifer forest with annual aboveground primary production of $\sim 1100 \text{ g m}^{-2} \text{ yr}^{-1}$ and near complete canopy cover at high elevation. Greater influx of organic materials into the mixed conifer system likely promotes enhanced silicate weathering via feldspar interaction with organic acids and ligands (Stillings et al., 1996). For example, feldspar weathering rates increase up to fifteen-fold in the presence of organic acids in laboratory experiments (Ullman et al., 1996; Welch and Ullman, 1996; Drever and Stillings, 1997). Additionally, feldspar weathering is also likely enhanced in the mixed conifer systems as a result of greater proton activity. Soil KCl pH values decrease from ~ 4.9 in the desert scrub system to ~ 4.3 in the

mixed conifer system indicating greater exchangeable acidity (Pionke and Corey, 1967; Ross, 1995). Greater exchangeable acidity in the mixed conifer location results from a combination of acidic conifer litter inputs that have pH values ~ 4.5 (Heckman et al., 2011), and enhanced loss of base cations due to greater water flux through the soil system (Moss and Edmunds, 1992). In particular, Whittaker et al. (1968) observed that surface soil base saturation decreased from 100% to $<40\%$ with increasing elevation across the SCM gradient indicating greater loss of non-hydrolyzing cations with increased water availability and primary production. Feldspar dissolution rates can increase by an order of magnitude when pH decreases from 5 to 3 (Sokolova, 2013). The observed increase of Na depletion in the mixed conifer sites is thus likely a function of both of greater water availability, and greater inputs of reduced carbon compounds and protons into the soil system.

4.1.2. Landscape position controls on plagioclase weathering

The bulk soil data also indicated significant control of landscape position on Na depletion. Both the desert scrub and mixed conifer sites exhibited greater Na depletion in the water gathering convergent positions with an increase in maximum convergent Na depletion from $\sim 15\%$ to 33% , respectively. In particular, the greatest Na depletion was observed in mixed conifer convergent landscapes (Fig. 4b), likely a result of both the water-gathering nature of this topographic position and the average annual excess of water in this system. In contrast, the water shedding divergent landscape positions in the desert scrub and mixed conifer systems exhibited less Na depletion with elevation, increasing from 5.4% to 16% , respectively. These data suggest that despite significant variation in climate and biological production across the environmental gradient, the local redistribution of water on the landscape may exert strong control on silicate weathering and Na depletion.

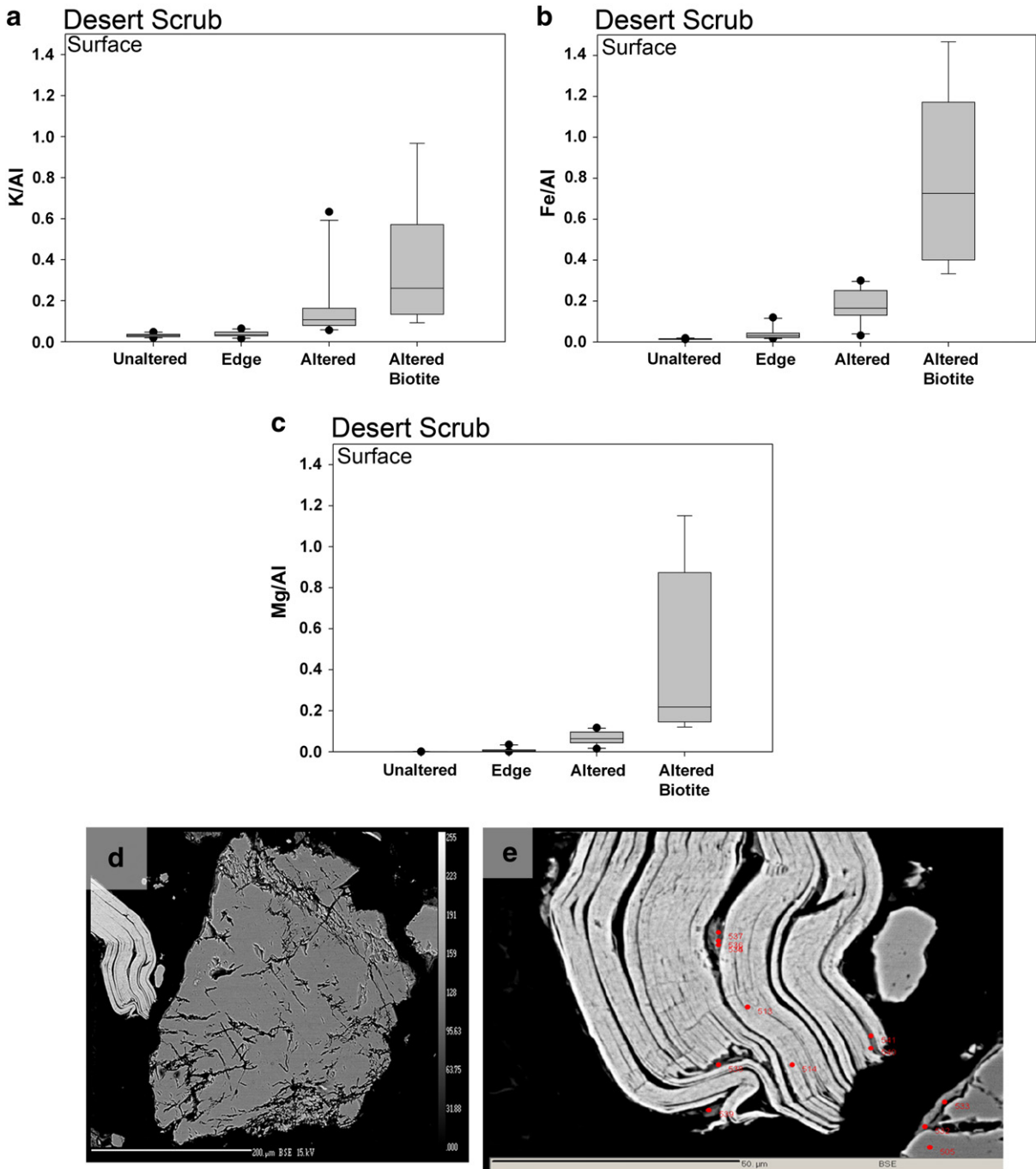


Fig. 9. Element ratios calculated for plagioclase grains in the desert scrub surface sample including a) K/Al, b) Fe/Al, and c) Mg/Al ratios. The microprobe point chemical analyses were performed on d) a biotite grain adjacent to a plagioclase grain included in the study with e) a magnified view of the transforming biotite grain containing red symbols where point analyses were taken.

Greater Na depletion in the water-gathering convergent landscape positions relative to upslope hillslope locations corresponds with the concept of a “leaching catena.” Here, a combination of overland and subsurface flow from upslope soils and increased downslope infiltration promotes greater silicate weathering and chemical depletion (Sommer and Schlichting, 1997).

4.2. Linking bulk soil chemical depletion to microscale weathering

4.2.1. Variation in plagioclase weathering

Differences in plagioclase transformation between the desert scrub and mixed conifer sites were recognized as elemental and textural differences at the feldspar–secondary mineral interface. Altered products

of the desert scrub plagioclase grains were limited to grain crevices, fractured edges, and clay coatings on grain exteriors (Figs. 3a, 10a–c). Similarly, Zhu et al. (2006) found that altered products from weathered feldspars in Navajo Sandstone from Black Mesa, AZ were contained predominately in grain cracks and cleavage planes. Altered products within the SCM desert scrub grain interiors were Si–Al rich and may be attributed to in situ plagioclase alteration. In comparison, the altered products coating the outer edges of plagioclase surface grains as clay films were enriched in K (Fig. 8a), possibly a translocated secondary product of biotite weathering (Fig. 9a–e).

The degree of plagioclase transformation in the mixed conifer soils was highly variable, ranging from grains demonstrating near complete pseudomorphic transformation to secondary products (Fig. 11b), to

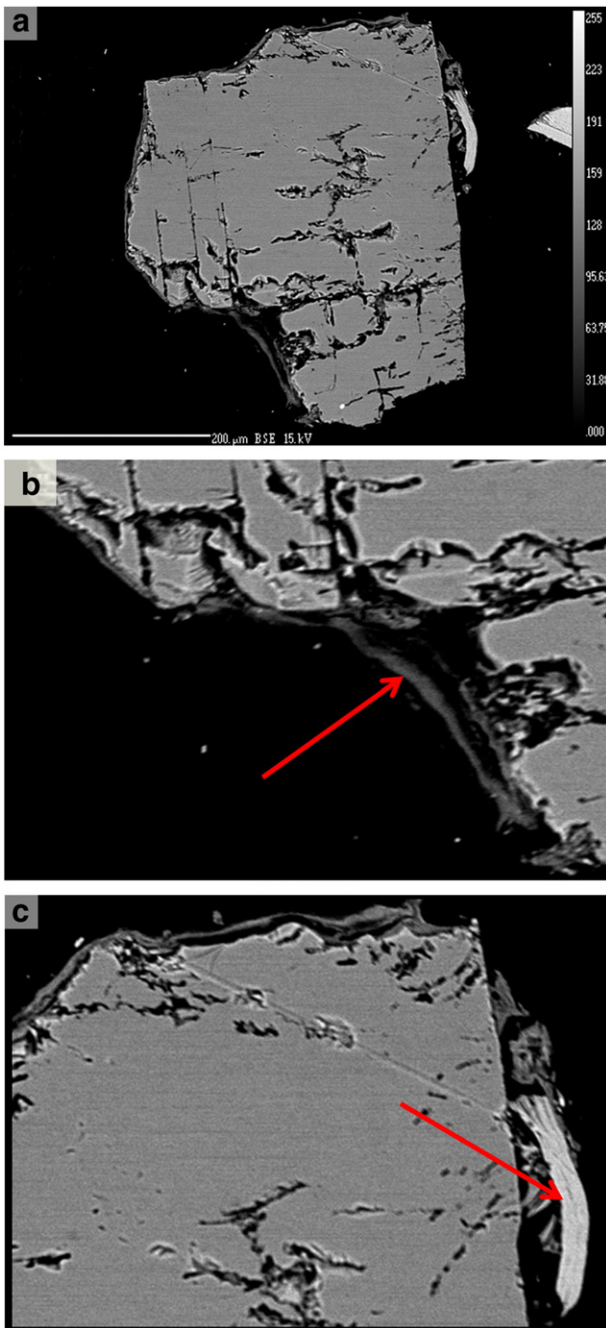


Fig. 10. Backscattered electron images of a) a desert scrub plagioclase feldspar b) containing thin, continuous clay films deposited along the edges of the entire grain. c) A small fragment of biotite is noted to the right of the grain.

grains exhibiting minimal weathering along grain cracks and fractures (Fig. 11a). The variable nature of plagioclase alteration in the more densely vegetated, relatively wet mixed conifer locations suggests an important role for intrinsic mineral resistance to alteration in mixed conifer semiarid environments. The smooth, more-intact plagioclase grains contained un-altered sections of plagioclase feldspar immediately adjacent to secondary weathering products similar to BSE imagery presented for transforming feldspars from temperate, granitic terrain in Portugal (Sequeira Braga et al., 2002). The altered plagioclase grain pictured in Fig. 11b reveals remnants of less altered sections enclosed by secondary weathering products, further suggesting grain-scale spatial variability in weathering resistance.

Similar to these observations, other studies of naturally weathered feldspars have observed areas of intense microscale feldspar grain

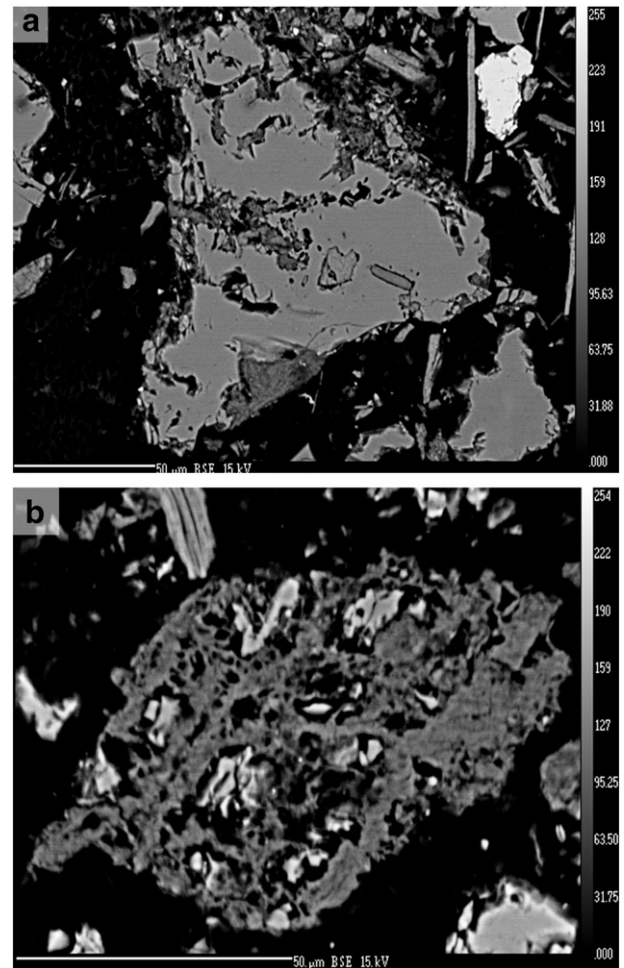


Fig. 11. The variability of mineral alteration in mixed conifer saprock is evident in two transforming plagioclase grains dominated by a) smooth, un-altered grain sections and b) darker, altered weathering products.

weathering adjacent to unweathered, clean feldspar surfaces (Wilson, 1975; Berner and Holdren, 1977; Wilson, 2004). These observations suggest that grain microtexture and dislocations may exert significant control on microscale weathering processes. In contrast, a lack of correlation between mineral dissolution and etch pit and/or dislocation densities in experimental studies brings into question the importance of etching in the weathering of feldspar (Holdren et al., 1988) and other minerals (Schott et al., 1989; Blum et al., 1990).

The relative degree of microtexture control on feldspar dissolution in field settings may be contingent on soil solution saturation state conditions (Lee et al., 1998). Three mineral dissolution mechanisms related to near-equilibrium, intermediate, and far-from equilibrium saturation states of the soil solution have been determined for calcite dissolution (Teng, 2004). The same mechanisms may also be applied to feldspars with the dominant feldspar dissolution mechanism depending on soil saturation state (Wilson, 2004). In general, near-equilibrium conditions yield minimal to no etch pit formation whereas far-from equilibrium conditions lead to an increase in “uncontrolled” etch pit formation at both grain dislocation zones and in defect-free zones (Teng, 2004). At intermediate saturation conditions, mineral dissolution occurs stepwise at microstructural grain defects and dislocation zones, emphasizing the role of mineral surface texture in controlling spatial patterns of mineral dissolution.

Based on the chemical changes documented for an extensive number of feldspar grains per soil sample, a relationship between microtexture and changes in elemental composition of feldspars at the grain scale appears rational, especially in the mixed conifer environment where

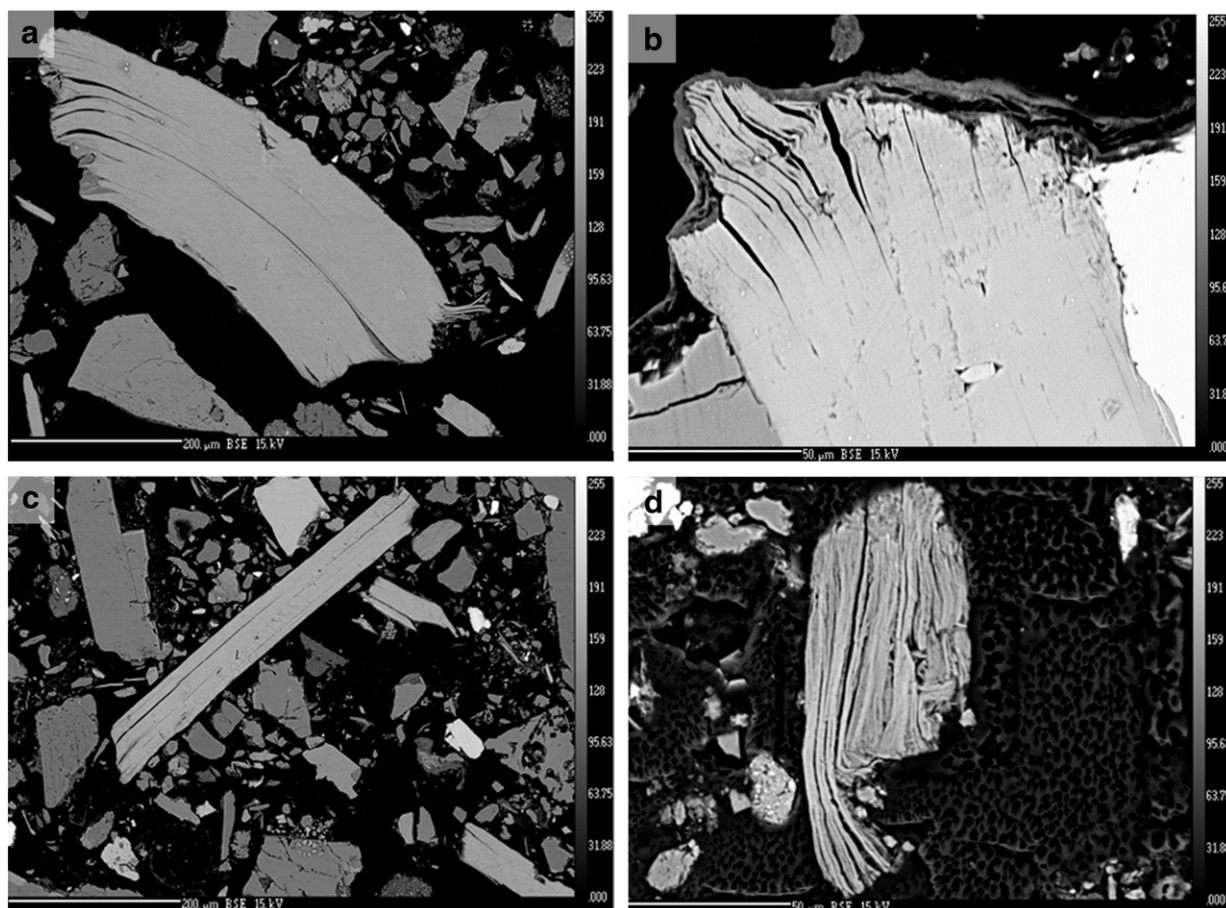


Fig. 12. Backscattered electron images depict frayed edge biotite alteration in desert scrub a) surface soil and b) saprock. c) Sand-sized biotite grains were also observed in the desert scrub surface soils and d) altered biotite was documented in desert scrub dust samples.

mineral transformations occur immediately adjacent to un-weathered sections of plagioclase grains (Fig. 3b). Etch pit formation was generally not observed in defect-free grain zones (Figs. 3a; 11a) but along grain dislocations or defects (Fig. 3b), as described for minerals in intermediate saturation states (Teng, 2004). Examining grain morphologies of both field sites revealed regions of un-weathered feldspar surfaces neighboring altered, Si and Al-rich secondary weathering products, suggesting that weaker grain sections are transformed before other, more chemically resistant grain areas.

4.2.2. Feldspar–secondary mineral interface

The complex mixture of weathered materials in the altered grain sections made the calculation of specific clay mineral formulas challenging. The Si/Al ratios of the mixed conifer altered products ranged from ~1 to 2, indicating a mixture of 1:1 and 2:1 phyllosilicate weathering products (Fig. 7c, d). The observed combination of secondary products suggests one proposed description of the crystalline feldspar–water interface where a thin (<10 nm), discontinuous layer of kaolinite is covered by an outer layer of precipitated smectite (Zhu et al., 2006). Both layers would have been encompassed by the 2 μm beam used in the current study. A complex mixture of secondary weathered products at the feldspar–secondary mineral interface would explain both variable Si/Al ratios (Fig. 7c, d) and well-constrained Na loss from unaltered/edge feldspar surfaces to altered products (Fig. 6c, d). The Si/Al ratios would be affected by the elements composing the altered products while Na loss would be expected in the formation of both kaolinite and smectite materials from transforming plagioclase grains.

4.3. Sources of elemental enrichment in desert scrub surface soils

The enrichment of K, Fe, and Mg in the plagioclase altered materials from the desert scrub surface soil (Figs. 6a; 7a) was unexpected and initiated speculation on possible controls of the observed elemental variability. The altered materials observed in the desert scrub surface soil were in the form of clay films rather than in situ alteration products, suggesting that the altered materials may in part derive from minerals other than the plagioclase. While the exact mechanism for this enrichment cannot be determined from the data collected, we hypothesize that dust deposition and/or the initial stages of in situ biotite weathering released K-enriched secondary products into the soil profile that were subsequently translocated and deposited onto adjacent plagioclase grains as clay coatings (Fig. 10a–b). In support of this hypothesis, medium sand-sized (>250 μm in diameter) frayed-edge biotite grains were observed in desert scrub surface soil and saprock samples (Fig. 12a, b), indicating the potential for K contribution to secondary phases from biotite alteration. Additionally, microprobe analyses of dust samples from this site confirmed the presence of altered biotite in the dust (Fig. 12d). The desert scrub soils were enriched in biotite relative to the parent rock indicating the possibility for dust contribution to the surface material. However, chemical distinction between dust-derived and in situ altered biotite mineral formula was not possible (Table 2). The evidence for both dust and parent material biotite weathering, combined with the morphology and chemistry of the altered materials, suggests that secondary biotite weathering products may in part contribute to the altered materials found on the plagioclase grains. However, as noted, alternative mechanisms of enrichment cannot be ruled out with the data collected.

5. Conclusions

Quantifying soil Na depletion and microscale plagioclase weathering patterns across a semiarid environmental gradient in southern Arizona revealed strong connections among climate and vegetation, landscape position, and silicate weathering. Both bulk soil Na depletion and Na loss across plagioclase feldspar grains increased from hot, water-limited desert scrub sites to cool, wet, biologically productive mixed conifer forest. The greatest Na depletion, both in bulk soils and at the microscale, occurred in the mixed conifer convergent positions. These findings suggest that localized concentrations of surface and subsurface water exerts strong control on silicate weathering, particularly in environments where annual precipitation exceeds annual evapotranspiration. Secondary weathering products were found adjacent to smooth, un-altered feldspar surfaces in the desert scrub and mixed conifer sites, suggesting a coupling of grain microtexture to mineral alteration. The results document an important link between bulk soil element loss and microscale weathering processes, with increased chemical depletion and mineral transformation in the mixed conifer ecosystems.

Acknowledgments

This research was funded by NSF EAR-1123454, NSF EAR/IF-0929850, and the national Critical Zone Observatory program via NSF EAR-0724958 and NSF EAR-0632516. The authors also thank Dr. Kenneth Domanik, Dr. S. Mercer Meding, Mary Kay Amistadi, Justine Mayo, Stephanie Castro, Christopher Clingsmith, and Andrew Martinez for laboratory and field assistance.

Appendix A. Supplementary data

Supplementary data to this article can be found online at <http://dx.doi.org/10.1016/j.chemgeo.2014.04.022>.

References

- Berner, R.A., Holdren, G.R., 1977. Mechanism of feldspar weathering: some observational evidence. *Geology* 5, 369.
- Berner, R.A., Holdren, G.R., 1979. Mechanism of feldspar weathering—II. Observations of feldspars from soils. *Geochim. Cosmochim. Acta* 43, 1173–1186.
- Birkeland, P.W., 1999. *Soils and Geomorphology*. Oxford University Press, New York.
- Bish, D.L., 1994. Quantitative X-ray diffraction analysis of soils. In: Amonette, J.E., Zelazny, L.W. (Eds.), *Quantitative Methods in Soil Mineralogy*. Soil Science Society of America, Madison, USA, pp. 267–295.
- Bish, D.L., Post, J.E., 1993. Quantitative mineralogical analysis using the Rietveld full-pattern fitting method. *Am. Mineral.* 78, 932–940.
- Blum, A.E., Stillings, L.L., 1995. Feldspar dissolution kinetics. In: White, A.E., Brantley, S.L. (Eds.), *Chemical Weathering Rates of Silicate Minerals*. Am. Rev. Mineral., pp. 463–481.
- Blum, A.E., Yund, R.A., Lasaga, A.C., 1990. The effect of dislocation density on the dissolution rate of quartz. *Geochim. Cosmochim. Acta* 54, 283–291.
- Budyko, M.I., 1974. *Climate and Life*. Academic Press, New York.
- Chorover, J., Troch, P.A., Rasmussen, C., Brooks, P.D., Pelletier, J.D., Breshears, D.D., Huxman, T.E., Kurc, S.A., Lohse, K.A., McIntosh, J.C., Meixner, T., Schaap, M.G., Litvak, M.E., Perdril, J., Harpold, A., Durcik, M., 2011. How water, carbon, and energy drive critical zone evolution: the Jemez–Santa Catalina critical zone observatory. *Vadose Zone J.* 10, 884–899.
- Churchman, G.J., Whitton, J.S., Claridge, G.G.C., Theng, B.K.G., 1984. Intercalation method using formamide for differentiating halloysite from kaolinite. *Clays Clay Miner.* 32, 241–248.
- Dahlgren, R.A., Boettinger, J.L., Huntington, G.L., Amundson, R.G., 1997. Soil development along an elevational transect in the western Sierra Nevada, California. *Geoderma* 78, 207–236.
- Dickinson, W.R., 1991. Tectonic setting of faulted Tertiary strata associated with the Catalina core complex in southern Arizona. *Geol. Soc. Am. Spec. Pap.* 264, 106.
- Dickinson, W.R., 2002. The Basin and Range province as a composite extensional domain. *Int. Geol. Rev.* 44, 1–38.
- Dixon, J.C., Campbell, S.W., Thorn, C.E., Darmody, R.G., 2006. Incipient weathering rind development on introduced machine-polished granite discs in an Arctic alpine environment, northern Scandinavia. *Earth Surf. Process. Landf.* 31, 111–121.
- Dixon, J.L., Heimsath, A.M., Amundson, R., 2009. The critical role of climate and saprolite weathering in landscape evolution. *Earth Surf. Process. Landf.* 34, 1507–1521.
- Downs, R.T., Hall-Wallace, M., 2003. *The American Mineralogy Crystal Structure Database*. *Am. Mineral.* 88, 247–250.
- Drever, J.I., Stillings, L.L., 1997. The role of organic acids in mineral weathering. *Colloids Surf. A* 120, 167–181.
- Driese, S.G., Medaris, L.G.J., Ren, M., Runkel, A.C., Langford, R.P., 2007. Differentiating pedogenesis from diagenesis in early terrestrial paleoweathering surfaces formed on granitic composition parent materials. *J. Geol.* 115, 387–406.
- Eberl, D., 2003. *User's Guide to ROCKJOCK – A Program for Determining Quantitative Mineralogy From Powder X-ray Diffraction Data*.
- Egli, M., Mirabella, A., Sartori, G., Fitze, P., 2003. Weathering rates as a function of climate: results from a climosequence of the Val Genova (Trentino, Italian Alps). *Geoderma* 111, 99–121.
- Fordham, A.W., 1990. Treatment of microanalyses of intimately mixed products of mica weathering. *Clays Clay Miner.* 38, 179–186.
- Ghabru, S.K., Mermut, A.R., St. Arnaud, R.J., 1987. The nature of weathered biotite in sand-sized fractions of Gray Luvisols (Boralfs) in Saskatchewan, Canada. *Geoderma* 40, 65–82.
- Graham, R.C., Rossi, A.M., Hubbert, K., 2010. Rock to regolith conversion: producing hospitable substrates for terrestrial ecosystems. *GSA Today* 20, 4–9.
- Green, E.G., Dietrich, W.E., Banfield, J.F., 2006. Quantification of chemical weathering rates across an actively eroding hillslope. *Earth Planet. Sci. Lett.* 242, 155–169.
- Heckman, K., Vazquez-Ortega, A., Gao, X., Chorover, J., Rasmussen, C., 2011. Changes in water extractable organic matter during incubation of forest floor material in the presence of quartz, goethite and gibbsite surfaces. *Geochim. Cosmochim. Acta* 75, 4295–4309.
- Heimsath, A.M., Dietrich, W.E., Nishiizumi, K., Finkel, R.C., 1997. The soil production function and landscape equilibrium. *Nature* 388, 358–361.
- Hellmann, R., Penisson, J.-M., Hervig, R.L., Thomassin, J.-H., Abrioux, M.-F., 2003. An EFTEM/HRTEM high-resolution study of the near surface of labradorite feldspar altered at acid pH: evidence for interfacial dissolution–reprecipitation. *Phys. Chem. Miner.* 30, 192–197.
- Hellmann, R., Wirth, R., Daval, D., Barnes, J.-P., Penisson, J.-M., Tisserand, D., Epicier, T., Florin, B., Hervig, R.L., 2012. Unifying natural and laboratory chemical weathering with interfacial dissolution–reprecipitation: a study based on the nanometer-scale chemistry of fluid–silicate interfaces. *Chem. Geol.* 294–295, 203–216.
- Hill, D., Sawhney, B., 1971. Electron microprobe analysis of soils. *Soil Sci.* 112, 32–38.
- Hochella, M.F., Banfield, J.F., 1995. Chemical weathering of silicates in nature: microscopic perspective with theoretical considerations. In: White, A.F., Brantley, S.L. (Eds.), *Chemical Weathering Rates of Silicate Minerals*. Mineralogical Society of America.
- Holdren, G.R., Casey, W.H., Westrich, H.R., Carr, M., Boslough, M., 1988. Bulk dislocation densities and dissolution rates in a calcic plagioclase. *Chem. Geol.* 70, 79.
- Huggett, R.J., 1975. Soil landscape systems: a model of soil genesis. *Geoderma* 13, 1–22.
- Jacobson, A.D., Blum, J.D., Chamberlain, C.P., Craw, D., Koons, P.O., 2003. Climatic and tectonic controls on chemical weathering in the New Zealand Southern Alps. *Geochim. Cosmochim. Acta* 67, 29–46.
- Jin, L., Ravella, R.R., Ketchum, B., Bierman, P.R., Heaney, P., White, T., Brantley, S.L., 2010. Mineral weathering and elemental transport during hillslope evolution at the Susquehanna/Shale Hills Critical Zone Observatory. *Geochim. Cosmochim. Acta* 74, 3669–3691.
- Kauffman, R.A., Van Dyk, D., 1994. Feldspars. In: Carr, D.D., et al. (Eds.), *Industrial Minerals and Rocks*, 6th edition. Soc. for Mining, Metallurgy, and Exploration, Inc., pp. 473–481.
- Khomo, L., Hartshorn, A.S., Rogers, K.H., Chadwick, O.A., 2011. Impact of rainfall and topography on the distribution of clays and major cations in granitic catenas of southern Africa. *Catena* 87, 119–128.
- Konen, M.E., Jacobs, P.M., Burras, C.L., Talaga, B.J., Mason, J.A., 2002. Equations for predicting soil organic carbon using loss-on-ignition for north central U.S. soils. *Soil Sci. Soc. Am. J.* 66, 1878–1881.
- Lagache, M., 1961. Dissolution des Feldspaths Alcalins Dans Leau Pure Ou Chargee De CO2 A 200 Degrees C. *C. R. Acad. Sci. Paris* 253, 2019–2022.
- Lee, M.R., Hodson, M.E., Parsons, I., 1998. Intragranular microtextures and microstructures in chemical and mechanical weathering: direct comparisons of experimentally and naturally weathered alkali feldspars. *Geochim. Cosmochim. Acta* 62, 2771–2788.
- Lee, M.R., Hodson, M.E., Brown, D.J., MacKenzie, M., Smith, C.L., 2008. The composition and crystallinity of the near-surface regions of weathered alkali feldspars. *Geochim. Cosmochim. Acta* 72, 4962–4975.
- Lybrand, R., Rasmussen, C., Jardine, A., Troch, P., Chorover, J., 2011. The effects of climate and landscape position on chemical denudation and mineral transformation in the Santa Catalina mountain critical zone observatory. *Appl. Geochem.* 26, S80–S84.
- Moore, D.M., Reynolds, R.C.J., 1997. *X-Ray Diffraction and the Identification and Analysis of Clay Minerals*. Oxford University Press, New York.
- Moss, Edmunds, 1992. Processes controlling acid attenuation in the unsaturated zone of a Triassic sandstone aquifer (U.K.), in the absence of carbonate minerals. *Appl. Geochem.* 7, 573–583.
- Moulton, K.L., West, J., Berner, R.A., 2000. Solute flux and mineral mass balance approaches to the quantification of plant effects on silicate weathering. *Am. J. Sci.* 300, 539–570.
- Muhs, D.R., 1982. The influence of topography on the spatial variability of soils in Mediterranean climates. In: Thorn, C.E. (Ed.), *Space and Time in Geomorphology*. George Allen and Unwin, pp. 269–284.
- NRC, 2001. *Basic Research Opportunities in Earth Sciences*. National Academies Press. National Research Council, Washington, DC.
- Paces, T., 1973. Steady-state kinetics and equilibrium between ground water and granitic rock. *Geochim. Cosmochim. Acta* 37, 2641–2663.
- Papoulias, D., Panayota, T.-K., Katagas, C., 2004. Progressive stages in the formation of kaolin minerals of different morphologies in the weathering of plagioclase. *Clays Clay Miner.* 52, 275–286.
- Pelletier, J.D., Barron-Gafford, G.A., Breshears, D.D., Brooks, P.D., Chorover, J., Durcik, M., Harman, C.J., Huxman, T.E., Lohse, K.A., Lybrand, R., Meixner, T., McIntosh, J.C., Papuga, S.A., Rasmussen, C., Schaap, M., Swetnam, T.L., Troch, P.A., 2013. Coevolution

- of nonlinear trends in vegetation, soils, and topography with elevation and slope aspect: a case study in the sky islands of southern Arizona. *J. Geophys. Res. Earth Surf.* 118, 741–758.
- Pionke, H.B., Corey, R.B., 1967. Relations between acidic aluminum and soil pH, clay, and organic matter. *Soil Sci. Soc. Am. Proc.* 31, 749–752.
- Plumper, O., Putnis, A., 2009. The complex hydrothermal history of granitic rocks: multiple feldspar replacement reactions under subsolidus conditions. *J. Petrol.* 50, 967–987.
- Porder, S., Hilley, G.E., Chadwick, O.A., 2007. Chemical weathering, mass loss, and dust inputs across a climate by time matrix in the Hawaiian Islands. *Earth Planet. Sci. Lett.* 258, 414–427.
- Rasmussen, C., Tabor, N.J., 2007. Applying a quantitative pedogenic energy model across a range of environmental gradients. *Soil Sci. Soc. Am. J.* 71, 1719–1729.
- Rasmussen, C., Dahlgren, R.A., Southard, R.J., 2010. Basalt weathering and pedogenesis across an environmental gradient in the southern Cascade Range, California, USA. *Geoderma* 154, 473–485.
- Rasmussen, C., Brantley, S., Richter, D., Blum, A., Dixon, J., White, A.F., 2011. Strong climate and tectonic control on plagioclase weathering in granitic terrain. *Earth Planet. Sci. Lett.* 301, 521–530.
- Reheis, M.C., Kihl, R., 1995. Dust deposition in southern Nevada and California, 1984–1989: relations to climate, source area, and source lithology. *J. Geophys. Res.* 100, 8893–8918.
- Riebe, C.S., Kirchner, J.W., Granger, D.E., Finkel, R.C., 2001. Strong tectonic and weak climatic control of long-term chemical weathering rates. *Geology* 29, 511–514.
- Riebe, C.S., Kirchner, J.W., Finkel, R.C., 2004. Erosional and climatic effects on long-term chemical weathering rates in granitic landscapes spanning diverse climate regimes. *Earth Planet. Sci. Lett.* 224, 547–562.
- Rietveld, H.M., 1969. A profile refinement method for nuclear and magnetic structures. *J. Appl. Crystallogr.* 2, 65–71.
- Robertson, I.D.M., Eggleton, R.A., 1991. Weathering of granitic muscovite to kaolinite and halloysite and of plagioclase-derived kaolinite to halloysite. *Clays Clay Miner.* 39, 113–126.
- Ross, D., 1995. Recommended soil tests for determining soil cation exchange capacity. In: Thomas Sims, J., Wolf, A. (Eds.), *Recommended Soil Testing Procedures for the Northeastern United States*. Northeast Regional Bulletin #493. Agricultural Experiment Station, University of Delaware, Newark, DE.
- Schoeneberger, P.J., Wysocki, D.A., Benham, E.C., 2011. *Field Book for Describing and Sampling Soils, Version 3.0*. Natural Resources Conservation Service, National Soil Survey Center, Lincoln, NE.
- Schott, J., Brantley, S., Crerar, D., Guy, C., Borcsik, M., Williame, C., 1989. Dissolution kinetics of strained calcite. *Geochim. Cosmochim. Acta* 53, 373–382.
- Sedov, S., Solleiro-Rebolledo, E., Fedick, S.L., Pi-Puig, T., Vallejo-Gomez, E., Flores-Delgado, M.D.L., 2008. Micromorphology of a soil catena in Yucatán: pedogenesis and geomorphological processes in a tropical karst landscape. In: Kapur, S., Stoops, G. (Eds.), *New Trends in Soil Micromorphology*. Springer-Verlag, Berlin, pp. 19–37.
- Sequeira Braga, M., Paquet, H., Begonha, A., 2002. Weathering of granites in a temperate climate (NW Portugal): granitic saprolites and arenization. *Catena* 49, 41–56.
- Soil Survey Staff, 2004. *Soil survey laboratory methods manual*. Soil Survey Investigations Report No. 42, Version 4.0 (Lincoln, NE).
- Soil Survey Staff, 2009. *Soil survey field and laboratory methods manual*. In: Burt, R. (Ed.), *Soil Survey Investigations Report No. 51, Version 1.0*. U.S. Department of Agriculture, Natural Resources Conservation Service.
- Sokolova, T.A., 2013. The destruction of quartz, amorphous silica minerals, and feldspars in model experiments and in soils: possible mechanisms, rates, and diagnostics (the analysis of literature). *Eurasian Soil Sci.* 1, 98–112.
- Sommer, M., Schlichting, E., 1997. Archetypes of catenas in respect to matter—a concept for structuring and grouping catenas. *Geoderma* 76, 1–33.
- Speakman, S.A., 2013. *An Introduction to Rietveld Refinement using PANalytical X'Pert HighScore Plus v2.2d*.
- Spear, F.S., 1993. *Metamorphic phase equilibria and pressure–temperature–time paths*. Mineralogical Society of America, Washington, D. C.
- Stillings, L.L., Drever, J.L., Brantley, S.L., Sun, Y., Oxburgh, R., 1996. Rates of feldspar dissolution at pH 3–7 with 0–8 M oxalic acid. *Chem. Geol.* 132, 79–89.
- Teng, H.H., 2004. Controls by saturation state on etch pit formation during calcite dissolution. *Geochim. Cosmochim. Acta* 68, 253–262.
- Ullman, W.J., Kirchman, D.L., Welch, S.A., Vandevivere, P., 1996. Laboratory evidence for microbially mediated silicate mineral dissolution in nature. *Chem. Geol.* 132, 11–17.
- Velde, B., 1984. Electron microprobe analysis of clay minerals. *Clay Miner.* 19, 243–247.
- Watson, J.P., 1964. A soil catena on granite in southern Rhodesia. *J. Soil Sci.* 15, 238–250.
- Welch, S.A., Ullman, W.J., 1996. Feldspar dissolution in acidic and organic solutions: compositional and pH dependence of dissolution rate. *Geochim. Cosmochim. Acta* 60, 2939–2948.
- West, A.J., Galy, A., Bickle, M., 2005. Tectonic and climatic controls on silicate weathering. *Earth Planet. Sci. Lett.* 235, 211–228.
- White, A., Brantley, S., 1995. Chemical weathering rates of silicate minerals; an overview. *Rev. Mineral. Geochem.* 31, 1–22.
- White, A.F., Brantley, S.L., 2003. The effect of time on the weathering of silicate minerals: why do weathering rates differ in the laboratory and field? *Chem. Geol.* 202, 479–506.
- White, A., Blum, A., Schulz, M., Bullen, T.D., Harden, J.W., Peterson, M.L., 1996. Weathering rates of a soil chronosequence on granitic alluvium: I. Quantification of mineralogical and surface area changes and calculation of primary silicate reaction rates. *Geochim. Cosmochim. Acta* 60, 2533–2550.
- White, A.F., Bullen, T.D., Schulz, M.S., Blum, A.E., Huntington, T.G., Peters, N.M., 2001. Differential rates of feldspar weathering in granitic regoliths. *Geochim. Cosmochim. Acta* 65, 847–869.
- Whittaker, R., Niering, W., 1965. Vegetation of the Santa Catalina Mountains, Arizona: a gradient analysis of the south slope. *Ecology* 46, 429–452.
- Whittaker, R.H., Buol, S.W., Niering, W.A., Havens, Y.H., 1968. A soil and vegetation pattern in the Santa Catalina Mountains, Arizona. *Soil Sci.* 105, 440–450.
- Whittaker, R.H., Niering, W.A., 1975. Vegetation of the Santa Catalina Mountains, Arizona. V. Biomass, Production, and Diversity along the Elevation Gradient. *Ecology* 56, 771–790.
- Williams, J.Z., Bandstra, J.Z., Pollard, D., Brantley, S.L., 2010. The temperature dependence of feldspar dissolution determined using a coupled weathering–climate model for Holocene-aged loess soils. *Geoderma* 156, 11–19.
- Wilson, M.J., 1975. Chemical weathering of some primary rock-forming minerals. *Soil Sci.* 119, 349–355.
- Wilson, M.J., 2004. Weathering of the primary rock-forming minerals: processes, products and rates. *Clay Miner.* 39, 233–266.
- Yoo, K., Mudd, S., 2008. Discrepancy between mineral residence time and soil age: implications for the interpretation of chemical weathering rates. *Geology* 36, 35–38.
- Yoo, K., Amundson, R., Heimsath, A.M., Dietrich, W.E., Brimhall, G.H., 2007. Integration of geochemical mass balance with sediment transport to calculate rates of soil chemical weathering and transport on hillslopes. *J. Geophys. Res.* 112, F02013.
- Young, R.A., 1993. *The Rietveld Method*. Oxford University Press, New York.
- Zhu, C., Veblen, D.R., Blum, A.E., Chipera, S.J., 2006. Naturally weathered feldspar surfaces in the Navajo Sandstone aquifer, Black Mesa, Arizona: electron microscopic characterization. *Geochim. Cosmochim. Acta* 70, 4600–4616.